electronics

Article

Novel Low-Loss Reverse-Conducting Insulated-Gate Bipolar Transitor with Collector-Side Injection-Enhanced Structure

Peijian Zhang [1], Sheng Qiu [2,3], Kunfeng Zhu [3,4] and Wensuo Chen [4,*]

1 Science and Technology on Analog Integrated Circuit Laboratory, Chongqing 400060, China
2 School of Integrated Circuit Science and Engineering, University of Electronic Science and Technology of China, Chengdu 610054, China
3 Sichuan Institute of Solid-State Circuits, Chongqing 400060, China
4 National Key Laboratory of Power Transmission Equipment Technology, School of Electrical Engineering, Chongqing University, Chongqing 400044, China
* Correspondence: wensuochen@cqu.edu.cn

Abstract: In this paper, a new concept of low-loss Reverse-Conducting Insulated-Gate Bipolar Transistor with Collector-side Injection-Enhanced structure (RC-IGBT-CIE) is proposed and investigated using simulations. In reverse conduction (the on state of the diode mode), the CIE structure enhances the collector-side carrier concentration of the proposed RC-IGBT-CIE, which results in low reverse-conducting voltage (V_F). The low reverse recovery loss and low turn-on loss using an inductive load circuit are obtained by using the modified carrier concentration profile resulted from both the CIE effect and the low-injection-efficiency p-emitter. Simulation results show that, with the same sum of turn-on loss and reverse recovery loss (E_{on} + E_{rec}), when compared to conventional RC-IGBT with anti-parallel thyristor (RC-IGBT-thyristor), the RC-IGBT-CIE reduces V_F by 9.2%, and meanwhile, with the same total conducting voltage ($V_{on,\, sat}$ + V_F), the total switching loss (E_{off} + E_{on} + E_{rec}) is reduced by 20.9% but does not sacrifice short-circuit capability.

Keywords: RC-IGBT; reverse recovery; reverse conduction; injection-enhanced; switching loss

check for updates

Citation: Zhang, P.; Qiu, S.; Zhu, K.; Chen, W. Novel Low-Loss Reverse-Conducting Insulated-Gate Bipolar Transitor with Collector-Side Injection-Enhanced Structure. *Electronics* **2024**, *13*, 23. https://doi.org/10.3390/electronics13010023

Academic Editors: Myounggon Kang and Min-Woo Kwon

Received: 5 November 2023
Revised: 14 December 2023
Accepted: 15 December 2023
Published: 20 December 2023

1. Introduction

Reverse-Conducting Insulated-Gate Bipolar Transistor (RC-IGBT) is a promising high-voltage power semiconductor device which integrates an IGBT and a freewheeling diode onto one chip to achieve both forward and reverse conductions [1–3]. RC-IGBTs can be used for many applications, such as in automotive motors and traction converters, etc. In these applications, the usual operating states of RC-IGBT include forward conduction (the on-state of the IGBT mode, referred to as the IGBT mode), reverse conduction (the on-state of the diode mode, referred to as the diode mode), forward turning-on (turning-on state of IGBT mode, referred to as turn-on mode), forward turning-off (the turning-off state of the IGBT mode, referred to as the turn-off mode) and reverse recovery (the reverse recovery state of the diode mode, referred to as the reverse recovery mode). Compared with the standard IGBT/diode two-chip approach, RC-IGBT increases power density, reduces the size of packages and greatly reduces the junction temperature ripples which leads to improved power-cycling capability. Yet, despite these benefits, it is difficult to optimize the same silicon for working in all operating states, which hampered the further application of RC-IGBT. The undesirable inherent snapback in the current–voltage characteristics (MOSFET-shorting effect in the collector side) of RC-IGBT, which makes it unsuitable for parallel operation, is the first and fundamental problem to be solved [4,5].

Fortunately, in recent years, many novel RC-IGBT structures have been proposed to suppress the snapback effect [6–24]. As detailed in [7], the simple collector shorting layout design, which provides a gradual decrease in the width of collector P+ from the center of the chip towards the outer edges while keeping a constant width of collector N+, can be used with RC-IGBT to eliminate the snapback effect. Additionally, the super-junction or semi-super-junction RC-IGBT was proposed to achieve snapback-free status by reducing the drift region resistance [8–10]. In [11,12], the high-resistance buffer layer was suggested to suppress the snapback effect. An actively controllable collector trench gate is employed in RC-IGBT, but it requires an additional complicated gate drive [13]. Some RC-IGBTs with collector trench are also proposed without additional control [14,15]. Other snapback-free RC-IGBTs, e.g., the collector P-floating [16–19], the N-Si/n-Ge heterojunction [20], and the P-drift [21], which utilize terminal region [22] and anti-parallel thyristor [23,24] are also reported in the literature.

Although these proposed structures suppress the snapback phenomenon within a small cell, they also bring a disadvantage, that is, they generally introduce a larger p-collector region next to the n-collector region in order to obtain a sufficient PN junction turning-on voltage (about 0.6–0.7 V for the silicon device), according to the snapback effect suppression mechanism [4]. In RC-IGBT reverse conduction, the reverse-biased p-collector/n-buffer junction leads to a relatively low carrier concentration near the collector side [5]. Meanwhile, a p-emitter with high injection efficiency is usually required in order to obtain a relatively low reverse conduction voltage drop [25,26]. Therefore, during reverse conduction, in these snapback-free RC-IGBT structures, the carrier concentration gradually decreases from the emitter side to the collector side. However, according to the mechanism of power diodes [27–31], this carrier concentration profile leads to poor reverse recovery performances, such as large peak reverse recovery current and long reverse recovery time. In RC-IGBT applications, it results in large reverse recovery loss (mainly from the reverse recovery mode) and large turn-on loss (mainly from the turn-on mode).

As a solution to the above problems, in this paper, a new concept of a 1.2 kV rated Collector-side Injection-Enhanced RC-IGBT structure (RC-IGBT-CIE) with a modified carrier concentration profile and low loss is proposed. The detailed operation mechanism and simulation results will be discussed in the following sections.

2. Device Structures and Operation

2.1. Proposed Device Structure

The schematic cross-sections of the proposed RC-IGBT with a Collector-side Injection-Enhanced structure (RC-IGBT-CIE) and conventional RC-IGBT with anti-parallel thyristor (RC-IGBT-thyristor) [5,23,24] are shown in Figure 1a,b. Both the structures introduce an anti-parallel thyristor as the internal integrated diode which is composed of the p-emitter (emitter-side P+ anode and P well), the Carrier Storage (CS) layer, the n-drift, the Filed Stop (FS) layer, the collector-side P-base and the collector-side N+ region. The collector-side P-base is a floating region, isolated from collector contact by a thin oxide layer. For both RC-IGBTs, the doping concentration of the emitter-side P+ anode is used to control the hole-injection efficiency during reverse conduction.

As shown in Figure 1a,b, compared with the conventional RC-IGBT-thyristor, besides the antiparallel thyristor, the new structure has a special collector-side injection-enhanced (CIE) design. The CIE structure in the novel device refers to an extension of the collector-side P-base, away from collector-side N+ (width of Lf), which is designed as a floating region by means of oxide layer isolation. The small Lf = 3 μm in the conventional RC-IGBT-thyristor is only there for the purpose of forming a floating p-base structure, and its injection enhancement effect can be ignored. Both of the proposed RC-IGBT-CIE and conventional RC-IGBT-thyristor have the same cell width of 30 μm and the same collector-side N+ width of 2 μm. For the RC-IGBT-thyristor, the width (Lc for short) of collector-side P+ is Lc = 25 μm. But, for the RC-IGBT-CIE, Lc changes as Lf changes, because the sum of the two (Lc + Lf) remains the same 28 μm. In the following discussion, we choose Lf as the variable, and if Lf is selected, Lc is fixed.

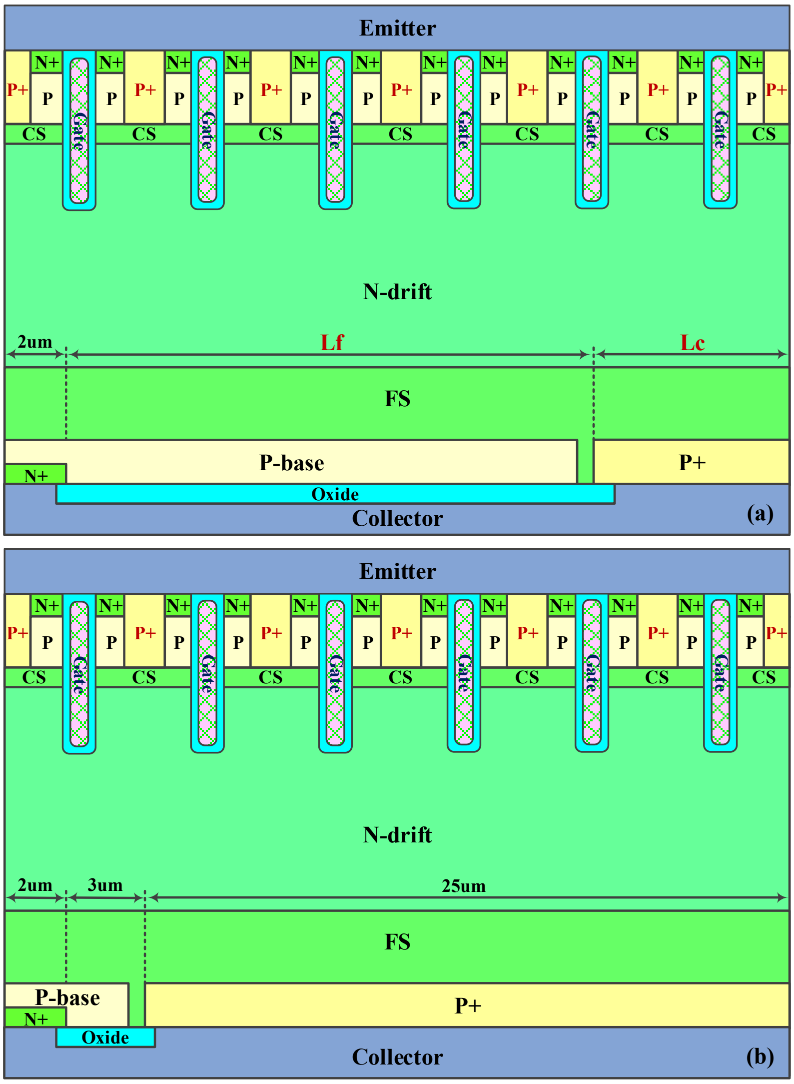

Figure 1. Schematic cross-sections of the cells of (**a**) proposed RC-IGBT-CIE and (**b**) conventional RC-IGBT-thyristor.

2.2. Collector-Side Injection-Enhanced Mechanism

The anti-parallel thyristor in both the novel RC-IGBT-CIE and conventional RC-IGBT-thyristor is introduced to suppress the snapback phenomenon in forward conduction (the on state of the IGBT mode). It is reported that the thyristor has a comparable conduction voltage to a PIN diode and it is triggered when either the NPN or PNP is operating in punch-through mode (either the n-drift/FS or the collector-side P-base is depleted) or when the current gains of the NPN and PNP transistors equal one [5,23,24]. In principle, the snapback-suppressed structure, anti-parallel thyristor or other structures do not affect the following discussion of how the CIE structure works.

2.2.1. Reverse Conduction State (Diode Mode)

The schematic collector-side carriers flow in reverse conduction state of the proposed RC-IGBT-CIE and conventional RC-IGBT-thyristor are shown in Figure 2a,b.

For the conventional RC-IGBT-thyristor, as shown in Figure 2b, in reverse conduction, the electrons which are injected from the N+ collector pass through the collector-side P-base, FS and n-drift regions, and eventually flow to the emitter side. And, holes which are injected from the p-emitter (emitter-side P+ anode and P well) eventually flow directly to the P+ collector. The large region of the collector-side reverse-biased P+/n-FS junction leads to a relatively low carrier concentration near the collector side [6].

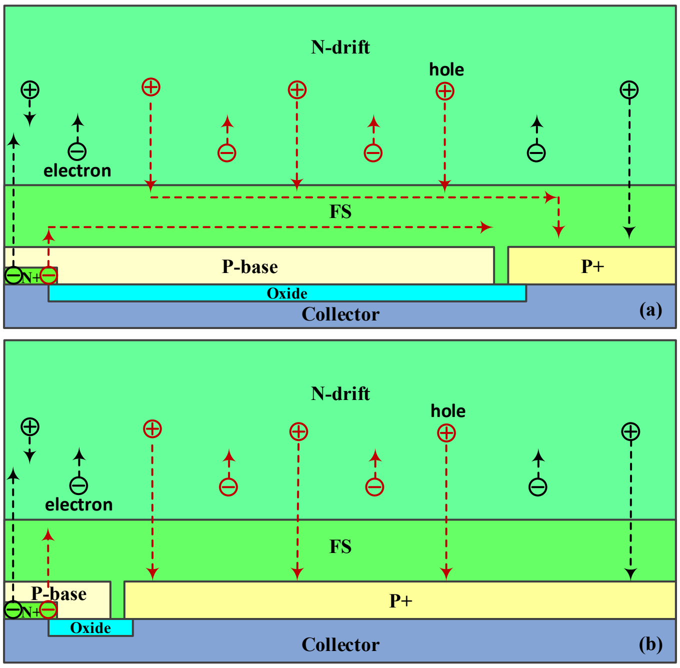

Figure 2. Schematic collector-side carriers flow in reverse conduction state (on-state of diode mode) of (**a**) proposed RC-IGBT-CIE and (**b**) conventional RC-IGBT-thyristor.

However, for the proposed RC-IGBT-CIE, as shown in Figure 2a, the holes which are injected from the p-emitter not only flow directly to the P+ collector, but also transversely over the large width of the floating collector P-base (CIE structure), resulting in a voltage drop, so that the electrons which are injected from the N+ collector are enhanced by the bias of the holes' lateral flow. The collector-side injection-enhanced effect of the proposed RC-IGBT-CIE in reverse conduction is similar to the operation mechanism of emitter-side injection-enhanced IGBT concept in forward conduction [32–34].

Besides the CIE effect, a modified carrier concentration distribution in RC-IGBT-CIE can be obtained by using a low-injection-efficiency p-emitter in reverse conduction. The reverse conduction carrier concentration distribution for the proposed RC-IGBT-CIE with different emitter-side P+ anode doping concentration (N_{PA}) and width of collector-side floating P-base (Lf) are shown in Figure 3. It can be seen that a lower N_{PA} results in a lower emitter-side carrier concentration, and a longer Lf results in higher collector-side carrier concentration. The variation of collector-side carrier concentration is mainly due to the CIE effect.

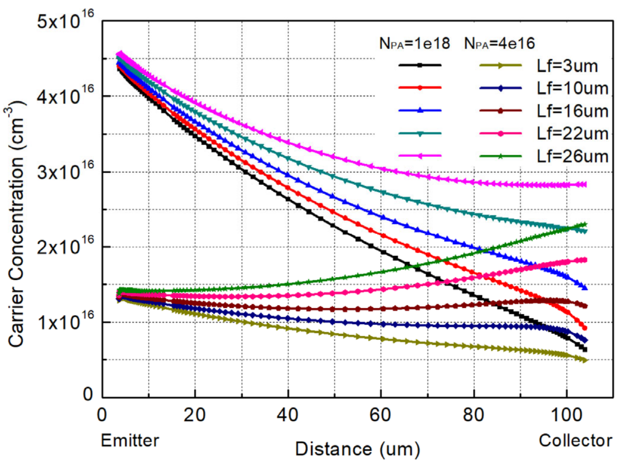

Figure 3. Reverse conduction carrier concentration for proposed RC-IGBT-CIE with different emitter-side P+ anode doping concentration (N_{PA}) and different width of collector-side floating P-base (Lf), temperature = 300 K.

Figure 4 shows the I–V curves of the reverse conduction (the on-state of the diode mode) for the proposed RC-IGBT-CIE with a different width of the collector-side floating P-base (Lf). It can be seen that, with the enhancement of CIE effect, the reverse-conducting voltage (V_F) gradually decreases, that is, Lf increases from small to large, resulting in the collector-side carrier concentration changing from low to high.

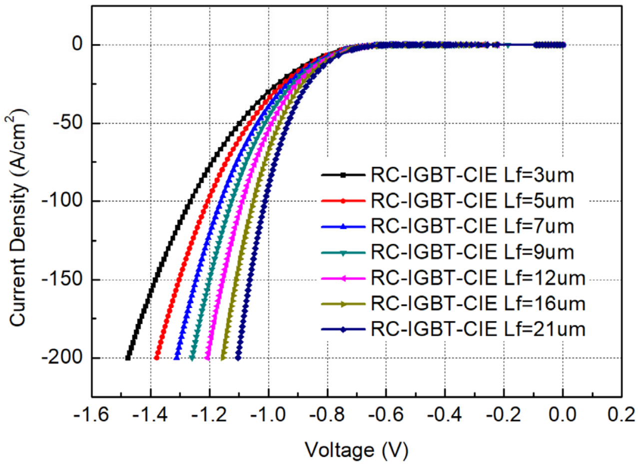

Figure 4. I–V curves of the reverse conduction (on-state of diode mode) for proposed RC-IGBT-CIE with fixed doping concentration of emitter-side P+ anode (N_{PA} = 4 × 10^{16} cm^{-3}) and different width of collector-side floating P-base (Lf), temperature = 300 K.

According to the operation mechanism of the power diodes [27–31], the peak reverse recovery current and reverse recovery time of a power diode depend very sensitively on the carrier concentration distribution of the conduction state. Therefore, the low reverse recovery loss (diode mode) and turn-on loss (IGBT mode) can be optimized for the proposed RC-IGBT-CIE because of the modified carrier concentration distribution in reverse conduction. The detailed discussion and simulation results' comparison will be presented in Section 3.

2.2.2. Forward Conduction State (IGBT Mode)

The schematic collector-side carriers that flow in the forward conduction state of the proposed RC-IGBT-CIE and conventional RC-IGBT-thyristor are shown in Figure 5a,b.

For the conventional RC-IGBT-thyristor, as shown in Figure 5b, in the forward conduction state, the holes which are injected from the P+ collector pass through the FS and n-drift regions, and eventually flow to the emitter side. Meanwhile, for the electrons which are injected from the n-emitter (emitter-side MOS channels), a few electrons directly pass through the collector-side P-base and flow to the N+ collector, and most electrons not only flow transversely over the large P+ collector to the N+ collector, but also reversely inject to the P+ collector. In the turn-on state (the turn-on state of the IGBT mode), the PN junction (P+ collector/n-FS) is turning on and the hole-injection from the P+ collector starts by providing sufficient bias for the above electron to transversely flow. This is the main effect of snapback suppression in the forward current–voltage characteristics of RC-IGBT.

However, for the proposed RC-IGBT-CIE, as shown in Figure 5a, in forward conduction state, most of the electrons reversely injecting to the P+ collector in the conventional RC-IGBT-thyristor case are gone because of the large collector-side floating P-base and are replaced transverse flow to the N+ collector, which results in an additional voltage drop, so that the holes which are injected from the P+ collector are enhanced by the additional bias of the electrons' lateral flow.

In general, the P+ collector impurity concentration of RC-IGBT is medium to high, so the electron reverse injection to the P+ collector is not very much. Therefore, the injection enhancement of the CIE structure on the forward conduction state is weak. The

CIE structure has a limited effect on the forward conduction, turn-off and the tradeoff relationship between turn-off loss (E_{off}) and forward saturation voltage ($V_{on,\,sat}$). These operation mechanisms will be verified by the simulation results in the following section.

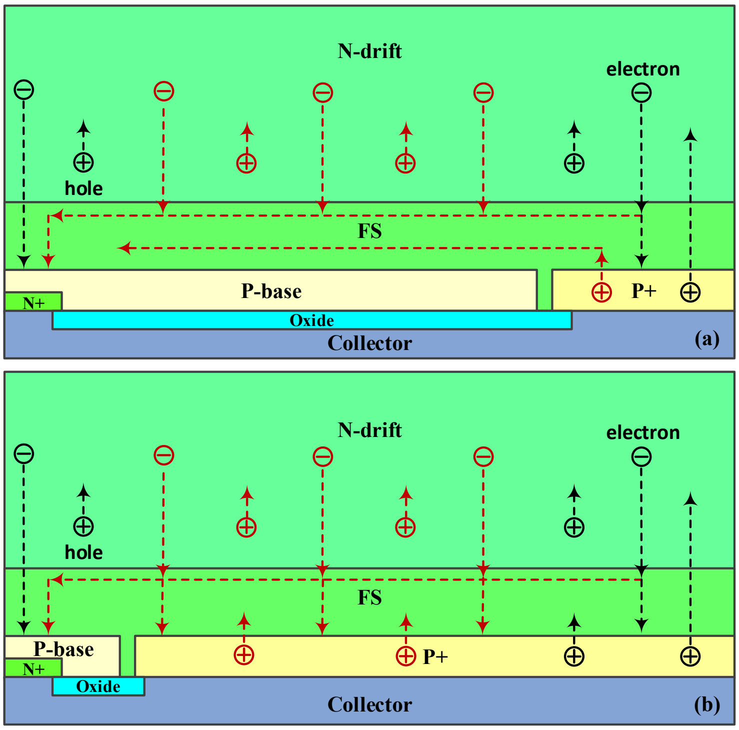

Figure 5. Schematic collector-side carriers flow in forward conduction state (on-state of IGBT mode) of (**a**) proposed RC-IGBT-CIE and (**b**) conventional RC-IGBT-thyristor.

3. Simulation Results and Discussion

In numerical simulation with a MEDICI simulator [35], the proposed RC-IGBT-CIE and conventional RC-IGBT-thyristor have the same structure except for the collector part. The main design parameters and their typical values are given in Table 1 and Figure 1a,b. During simulation, the key physical attributes modeled include barrier lowering, carrier mobility, Shockley–Read–Hall recombination, Auger recombination, band gap narrowing, carrier generation and impact ionization.

Table 1. Some of the design parameters and their typical values.

Design Parameters	RC-IGBT-CIE	RC-IGBT-Thyristor
silicon thickness (µm)	110	110
trench depth (µm)	6	6
gate oxide thickness (µm)	0.1	0.1
trench width (µm)	1	1
trench cell width (µm)	5	5
collector P+ width, Lc (µm)	16	25
collector floating P-base width, Lf (µm)	12	3
collector P+ depth (µm)	0.8	0.8
collector N+ depth (µm)	0.3	0.3
emitter P doping (cm^{-3})	3.2×10^{17}	3.2×10^{17}
collector P-base doping (cm^{-3})	1.5×10^{16}	1.5×10^{16}
emitter CS-layer doping (cm^{-3})	2×10^{16}	2×10^{16}
emitter P+ Anode doping, N_{PA} (cm^{-3})	4×10^{16}	4×10^{17}
collector P+ doping, N_{PC} (cm^{-3})	3.5×10^{17}	5×10^{17}
lifetime of carriers (µs)	2	2

3.1. *Simulation Results' Comparison and Discussion*

3.1.1. Static Characteristics Comparison

Figure 6a–c show the static characteristics comparison for the proposed RC-IGBT-CIE and conventional RC-IGBT-thyristor.

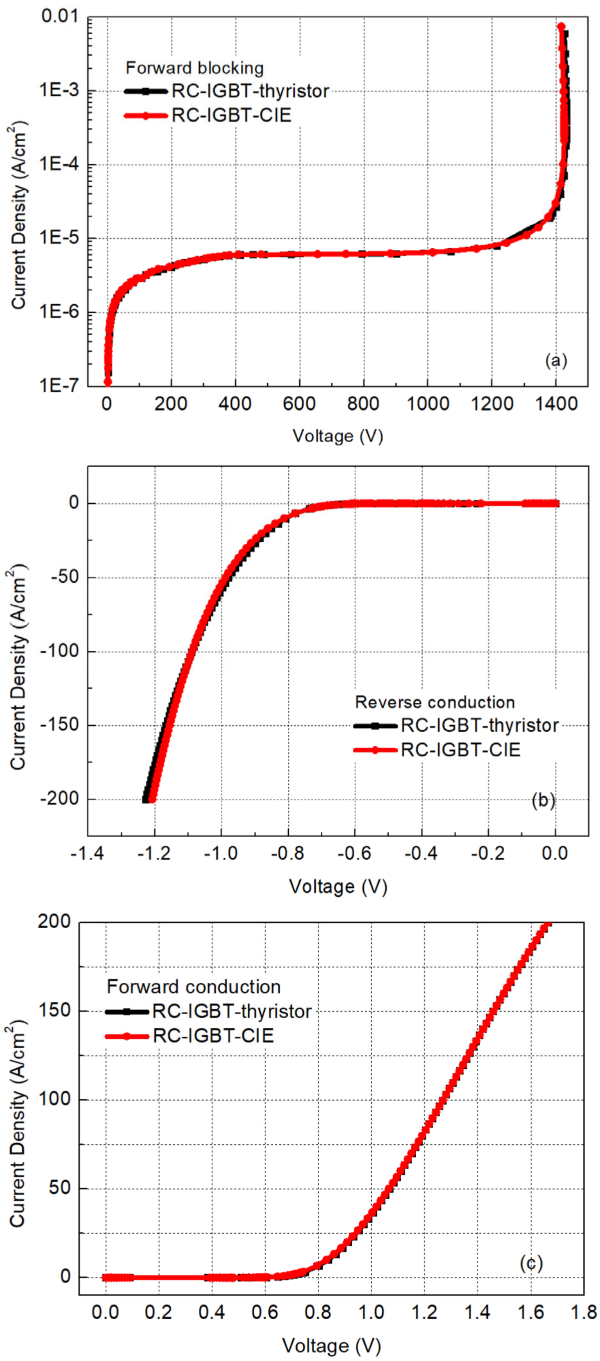

Figure 6. Static characteristics comparison for the proposed RC-IGBT-CIE and conventional RC-IGBT-thyristor, (**a**) I–V curves of the forward blocking, (**b**) I–V curves of the reverse conduction, and (**c**) I–V curves of the forward conduction, temperature = 300 K.

As shown in Figure 6a, for the I–V curves of the forward-blocking comparison, the two RC-IGBTs have almost the same forward-blocking characteristics and the breakdown voltages are larger than 1400 V. The CIE structure design does not affect the forward blocking characteristics.

In the following discussion, for ease of comparison, we usually make different RC-IGBTs have almost the same static characteristics (such as reverse conduction and forward conduction), and then compare their switching performances (such as reverse recovery, turn-on and turn-off).

As shown in Figure 6b, for the I–V curves of reverse conduction comparisons, based on the effect of the collector-side injection-enhanced mechanism on the reverse conduction discussed in the last section, by adjusting the emitter-side P+ anode doping concentration (N_{PA}) and the width of the collector-side floating P-base (Lf), the two RC-IGBTs have almost the same reverse conduction characteristics. For the proposed RC-IGBT-CIE, the $N_{PA} = 4 \times 10^{16}$ cm^{-3} and Lf = 12 µm are needed to make it have the same reverse conduction performance as that of the conventional RC-IGBT-thyristor with $N_{PA} = 4 \times 10^{17}$ cm^{-3}.

As shown in Figure 6c, for the I–V curves of forward conduction comparisons, the two RC-IGBTs have almost the same forward conduction characteristics. Based on the weak effect of the collector-side injection-enhanced mechanism on the forward conduction, for the proposed RC-IGBT-CIE, the P+ collector doping concentration $N_{PC} = 3.5 \times 10^{17}$ cm^{-3} is needed to make it have the same forward conduction performance as that of the conventional RC-IGBT-thyristor with $N_{PC} = 5 \times 10^{17}$ cm^{-3}.

Figure 7 shows the reverse conduction and forward conduction carrier concentration distributions for the proposed RC-IGBT-CIE and conventional RC-IGBT-thyristor. As seen, the two RC-IGBTs have almost the same forward conduction carrier concentration distribution. The collector-side carrier concentration is greater than that of the emitter-side because the two RC-IGBTs both adopt an emitter-side injection-enhanced structure as shown in Figure 1. However, for reverse conduction, the carrier concentration distribution of the two RC-IGBTs is obviously different. The emitter-side carrier concentration of the proposed RC-IGBT-CIE is much lower than that of the conventional RC-IGBT-thyristor, while the collector-side carrier concentration is higher than that of the conventional RC-IGBT-thyristor. These carrier concentration distributions conform to the collector-side injection-enhanced mechanism given in the previous section.

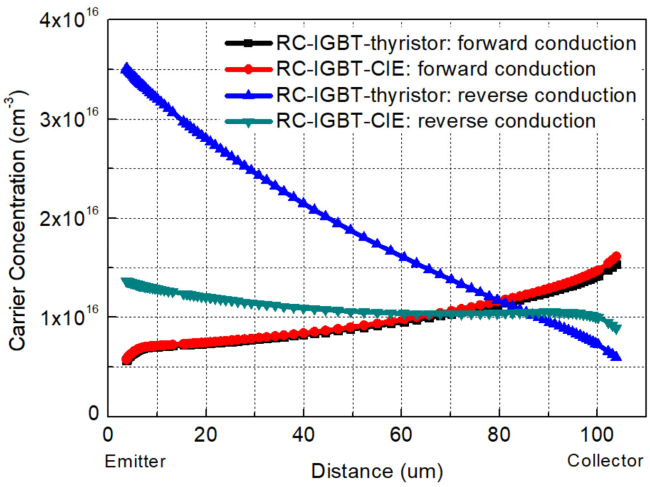

Figure 7. Reverse conduction (on-state of diode mode) and forward conduction (on-state of IGBT mode) carrier concentration for proposed RC-IGBT-CIE and conventional RC-IGBT-thyristor, temperature = 300 K.

3.1.2. Switching Characteristics Comparison

Figure 8 shows the inductive load circuit for transient analysis. The gate resistor (Rg) of 10 Ω and the stray inductance (Ls) of 120 nH are used. The switching current is 100 A in simulation. DUT1 and DUT2 are identical except for the gate control voltage.

Figure 9a–c show the switching characteristics comparison for the proposed RC-IGBT-CIE and conventional RC-IGBT-thyristor.

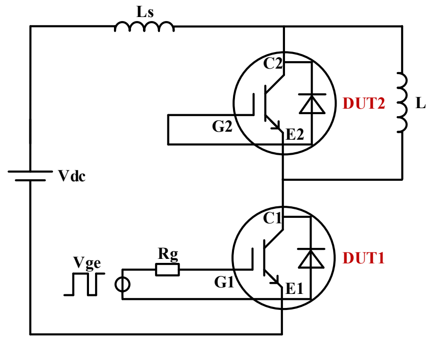

Figure 8. Inductive load circuit for transient analysis. The gate resistor (Rg) of 10 Ω and the stray inductance (Ls) of 120 nH are used.

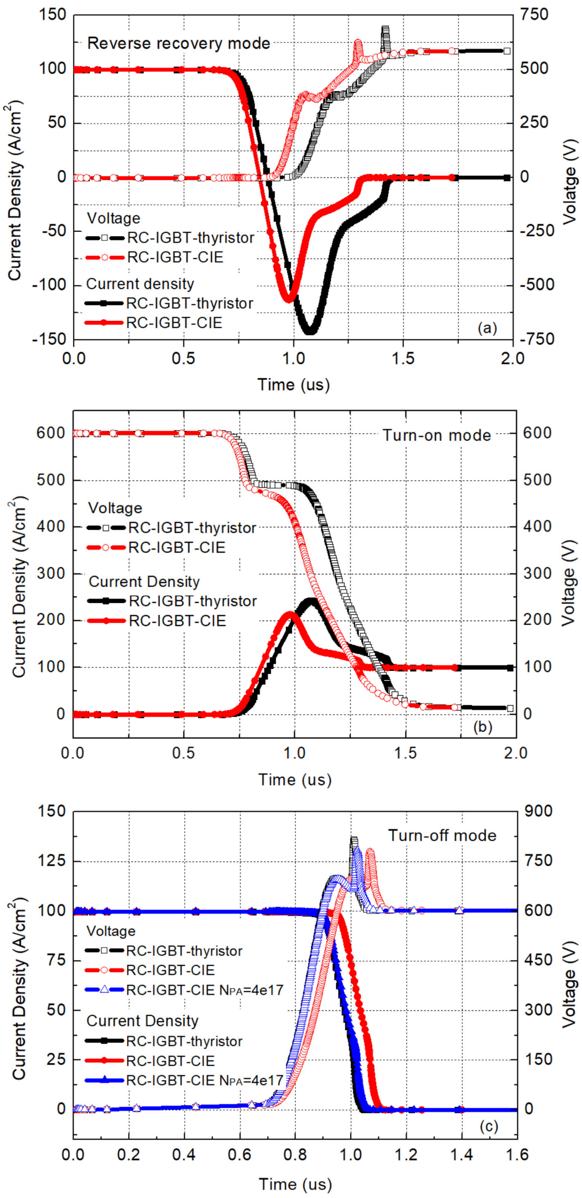

Figure 9. Switching characteristics comparison for the proposed RC-IGBT-CIE and conventional RC-IGBT-thyristor, (**a**) reverse recovery voltage and current density waveforms, (**b**) turn-on voltage and current density waveforms, and (**c**) turn-off voltage and current density waveforms, temperature = 300 K.

Figure 9a shows the reverse recovery voltage and current density waveforms for the proposed RC-IGBT-CIE and conventional RC-IGBT-thyristor. Compared with the conventional RC-IGBT-thyristor, the smaller peak reverse recovery current density and shorter reverse recovery time are obtained for the proposed RC-IGBT-CIE because of the modified carrier concentration distribution in the reverse conduction state which were discussed in the last section.

Figure 9b shows the turn-on voltage and current density waveforms for the proposed RC-IGBT-CIE and conventional RC-IGBT-thyristor. The proposed RC-IGBT-CIE has a smaller turning-on current density (the IGBT mode of DUT1, as shown in Figure 10) because of the smaller reverse recovery current density (the diode mode of DUT2, as shown in Figure 10).

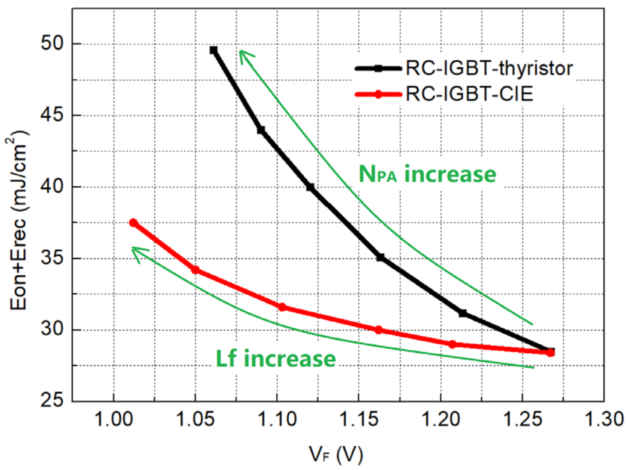

Figure 10. Reverse-conducting voltage (V_F) and the sum of turn-on loss and reverse recovery loss (E_{on} + E_{rec}) for proposed RC-IGBT-CIE obtained by varying the width of collector-side floating P-base (Lf), and for conventional RC-IGBT-thyristor obtained by varying the emitter-side P+ anode doping concentration (N_{PA}), temperature = 300 K.

Figure 9c shows the turn-off voltage and current density waveforms for the proposed RC-IGBT-CIE and conventional RC-IGBT-thyristor. When compared with conventional RC-IGBT-thyristor, the proposed RC-IGBT-CIE exhibits a slow turn-off speed but low recovery voltage peak. As the basic structure, the proposed RC-IGBT-CIE and conventional RC-IGBT-thyristor have emitter-side P+ anode doping concentration (N_{PA}) values of 4×10^{16} cm^{-3} and 4×10^{17} cm^{-3}, respectively, as shown in Table 1. For comparison, the turn-off voltage and current waveforms for the RC-IGBT-CIE with $N_{PA} = 4 \times 10^{17}$ cm^{-3} are also given.

In general, the turn-off process of the RC-IGBT depends on the disappearance of the electron–hole pairs generated by the conductance modulation effect of the forward conduction. As shown in Figure 9, both of the proposed RC-IGBT-CIE and conventional RC-IGBT-thyristor have almost the same carrier concentration distribution in the forward conduction state (the on-state of the IGBT mode). Therefore, the difference in emitter and collector structures of the RC-IGBT-CIE and RC-IGBT-thyristor is the influencing factor leading to different turn-off curves. Specifically, the voltage rise stage is mainly affected by the emitter structural parameter N_{PA}. The smaller the N_{PA} is, the slower the hole is extracted out. Therefore, the slower the depletion region is formed in the N-drift region and the slower the voltage rise, which can be seen from the comparison of the curves of the basic RC-IGBT-CIE ($N_{PA} = 4 \times 10^{16}$ cm^{-3}) and RC-IGBT-CIE with $N_{PA} = 4 \times 10^{17}$ cm^{-3}. The current downstage is mainly affected by the collector structure; the loss of electrons reversely injecting to the P+ collector slows down the electron extraction, so the current turn-off is slower, resulting in a lower recovery voltage peak. The effect of electrons reversely injecting to the P+ collector is weak, and its effect on the turn-off characteristics is limited, which is consistent with the discussion in Section 2.

3.2. Influences of Key Parameter on Operation and Tradeoff Curves

3.2.1. Influences of Key Parameter on Operation

For the proposed RC-IGBT-CIE, the width of the collector-side floating P-base (Lf) is one of the key parameters which significantly affects device characteristics.

Figure 10 shows the reverse-conducting voltage (V_F) and the sum of turn-on loss and reverse recovery loss ($E_{on} + E_{rec}$) for the proposed RC-IGBT-CIE obtained by varying the Lf, and for the conventional RC-IGBT-thyristor obtained by varying the emitter-side P+ anode doping concentration (N_{PA}), respectively. As seen, a smaller reverse-conducting voltage (V_F) means a larger change in the carrier concentration distribution of the reverse conduction state (the on state of the diode mode), that is, a faster carrier concentration decrease from the emitter side to the collector side for the conventional RC-IGBT-thyristor and a slower carrier concentration decrease from the emitter side to the collector side or a faster increase carrier concentration decrease from the emitter side to the collector side for the proposed RC-IGBT-CIE, as shown in Figure 3. The CIE effect brings a smaller V_F with the same sum of turn-on loss and reverse recovery loss ($E_{on} + E_{rec}$). Generally speaking, for the proposed RC-IGBT-CIE, the larger the N_{PA} is, the higher the emitter-side carrier concentration is. The larger Lf is, the stronger the collector-side enhancement effect is, and the higher the collector-side carrier concentration can be obtained. Therefore, according to the previous discussion, the smaller the N_{PA} is and/or the larger the Lf is, the better the carrier concentration distribution in reverse conduction is, which can better improve the device performance. In simulation, for the proposed RC-IGBT-CIE, $N_{PA} = 4 \times 10^{16}$ cm^{-3} is selected, which is the relatively low impurity concentration that can be achieved in the process. At the same time, Lf = 12 μm is selected, which helps the proposed RC-IGBT-CIE obtain almost the same reverse conduction I–V curve as the conventional RC-IGBT-thyristor. The switching characteristics are then compared and the tradeoff curves obtained to demonstrate the performance advantages of the new device, which is discussed in the next section.

3.2.2. Tradeoff Curves

Figure 11a–d show the tradeoff relationships for the proposed RC-IGBT-CIE and conventional RC-IGBT-thyristor.

Figure 11a shows the tradeoff relationship between turn-off loss (E_{off}) and forward saturation voltage ($V_{on,\,sat}$) obtained by varying P+ collector doping concentration (N_{PC}) for the proposed RC-IGBT-CIE and conventional RC-IGBT-thyristor. As discussed in the last section, the difference in the emitter and collector structures of RC-IGBT-CIE and RC-IGBT-thyristor is the influencing factor leading to different tradeoff curves, and the effect of the new structure on the tradeoff curve is limited, as seen from this figure.

Figure 11b shows the tradeoff relationship between reverse recovery loss (E_{rec}) and reverse-conducting voltage (V_F) obtained by varying the emitter-side P+ anode doping concentration (N_{PA}) for the proposed RC-IGBT-CIE and conventional RC-IGBT-thyristor. And, Figure 11c shows the tradeoff relationship between sum of turn-on loss and reverse recovery loss ($E_{on} + E_{rec}$) and V_F obtained by varying the N_{PA} for the proposed RC-IGBT-CIE and conventional RC-IGBT-thyristor. By comparing Figure 11b,c, we can see that the new structure has a significant impact on both E_{on} and E_{rec}. As seen from Figure 11c, when compared to the conventional RC-IGBT-thyristor, with the same sum of ($E_{on} + E_{rec}$), the V_f decreases by 9.2%.

Figure 11d shows the tradeoff relationship between sum of ($E_{off} + E_{on} + E_{rec}$) and sum of ($V_{on,\,sat} + V_F$) obtained by varying the N_{PA} for the proposed RC-IGBT-CIE and conventional RC-IGBT-thyristor. As seen, when compared to the conventional RC-IGBT-thyristor, with the same total conducting voltage ($V_{on,\,sat} + V_F$), the total switching loss for the proposed RC-IGBT-CIE ($E_{off} + E_{on} + E_{rec}$) decreases by 20.9%. It should be pointed out that the design parameter values of the two comparison points are shown in Table 1.

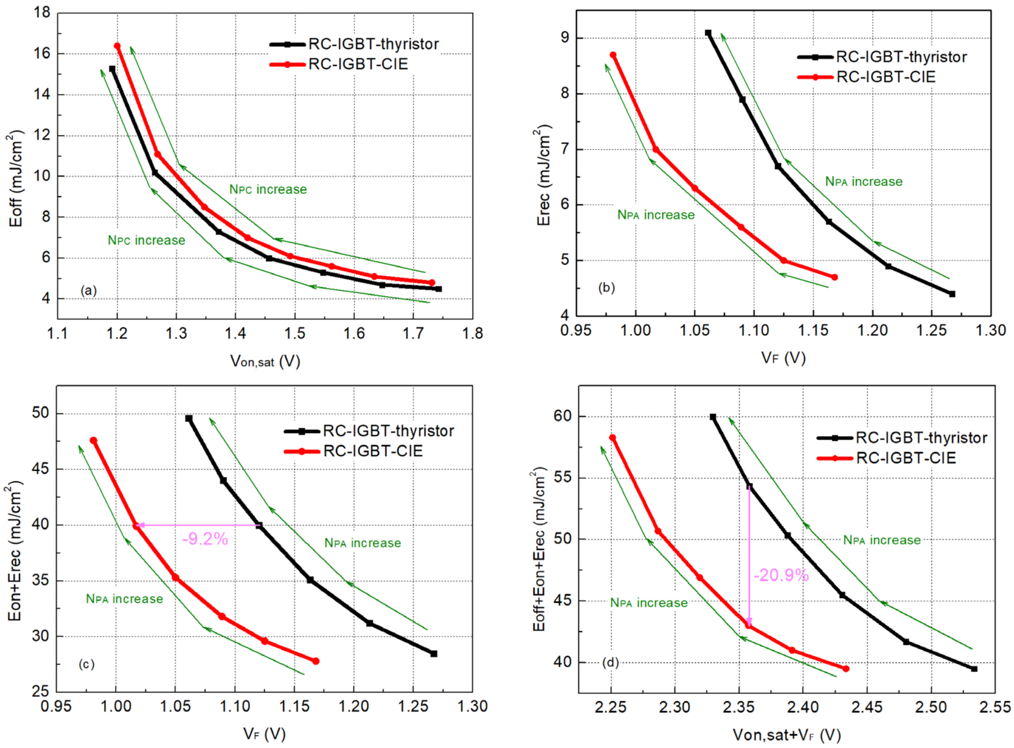

Figure 11. Tradeoff relationship for the proposed RC-IGBT-CIE and conventional RC-IGBT-thyristor: (**a**) between turn-off loss (E_{off}) and forward saturation voltage ($V_{on,\ sat}$), obtained by varying the P+ collector doping concentration (N_{PC}); (**b**) between reverse recovery loss (E_{rec}) and reverse-conducting voltage (V_f) obtained by varying the emitter-side P+ anode doping concentration (N_{PA}); (**c**) between sum of turn-on loss and reverse recovery loss (E_{on} + E_{rec}) and V_f obtained by varying the N_{PA}; and (**d**) between sum of turn-off loss, turn-on loss and reverse recovery loss (E_{off} + E_{on} + E_{rec}) and sum of ($V_{on,\ sat}$ + V_F), obtained by varying the N_{PA}; temperature = 300 K.

3.3. Short-Circuit Capability

Figure 12 shows the short circuit current waveforms (on-state of IGBT mode). Both of the proposed RC-IGBT-CIE and conventional RC-IGBT-thyristor have the same design parameters except for the width of collector-side floating P-base (Lf). Lf is 25 µm for the conventional RC-IGBT-thyristor and 16 µm for the proposed RC-IGBT-CIE. As seen, both of these RC-IGBTs can turn off the short-circuit current within 10 µs.

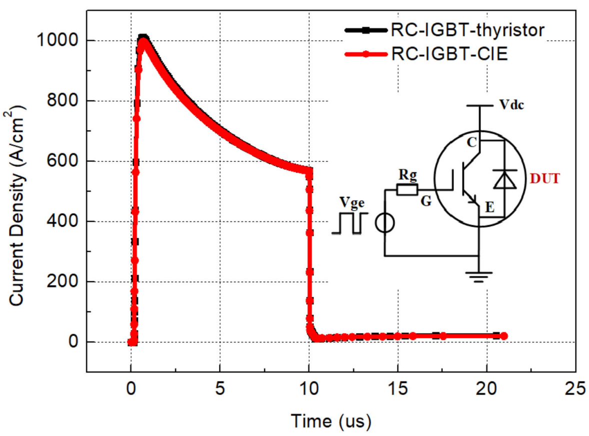

Figure 12. Short-circuit current waveforms (on state of IGBT mode). Both of the proposed RC-IGBT-CIE and conventional RC-IGBT-thyristor have the same design parameters except for the width of collector-side floating P-base (Lf), where Lf is 25 µm for the conventional RC-IGBT-thyristor and 16 µm for the proposed RC-IGBT-CIE, temperature = 300 K.

3.4. Fabrication and Thermal Resistivity Discussion

Both the proposed RC-IGBT-CIE and conventional RC-IGBT-thyristor can be fabricated by means of thin-wafer processing. The collector-side oxide layer is used only to isolate the current to the electrode and has no high electric field in itself or its adjacent silicon structure. So, the thickness can be made very thin. Therefore, its effect on thermal resistance may be very small. In process manufacturing, the collector-side thin oxide layer can be formed through the deposition process as low as 300 degrees Celsius.

4. Applicability Discussion

In the last two sections, we analyzed the operational mechanism of the proposed RC-IGBT-CIE and verified it by simulation analysis. In principle, not limited to the snapback-free RC-IGBT-thyristor, the CIE effect can be introduced into every RC-IGBT structure, with a mechanism similar to the above discussion of how the CIE structure works. To our knowledge, the structure proposed in this paper differs from other existing published RC-IGBTs in that it improves device performance by introducing a collector-side injection-enhancement effect. Among the many RC-IGBTs that have been published, the structure that is more similar to the new structure in this paper is the RC-IGBT with a floating P-region in the trench collector (RC-IGBT-PF for short in this paper) described in reference [16]. Figure 13 shows the static and switching characteristics comparison of forward conduction, reverse conduction, turn-off voltage and current density waveforms and reverse recovery current density waveforms for the proposed RC-IGBT-CIE, conventional RC-IGBT-thyristor and RC-IGBT-PF. Except for the N_{PA} and collector structure, all the RC-IGBTs in simulation have the same structure parameters. For the RC-IGBT-PF [16], N_{PA} = 6.5 $\times$ 10^{17} cm^{-3}, N_{PC} = 3.2 $\times$ 10^{17} cm^{-3}, the width of P-float region is 4.3 µm and the width of the gap of P-float is 0.7 µm. As seen, compared to the conventional RC-IGBT-thyristor and RC-IGBT-PF, the proposed RC-IGBT-CIE has an improvement in reverse characteristics.

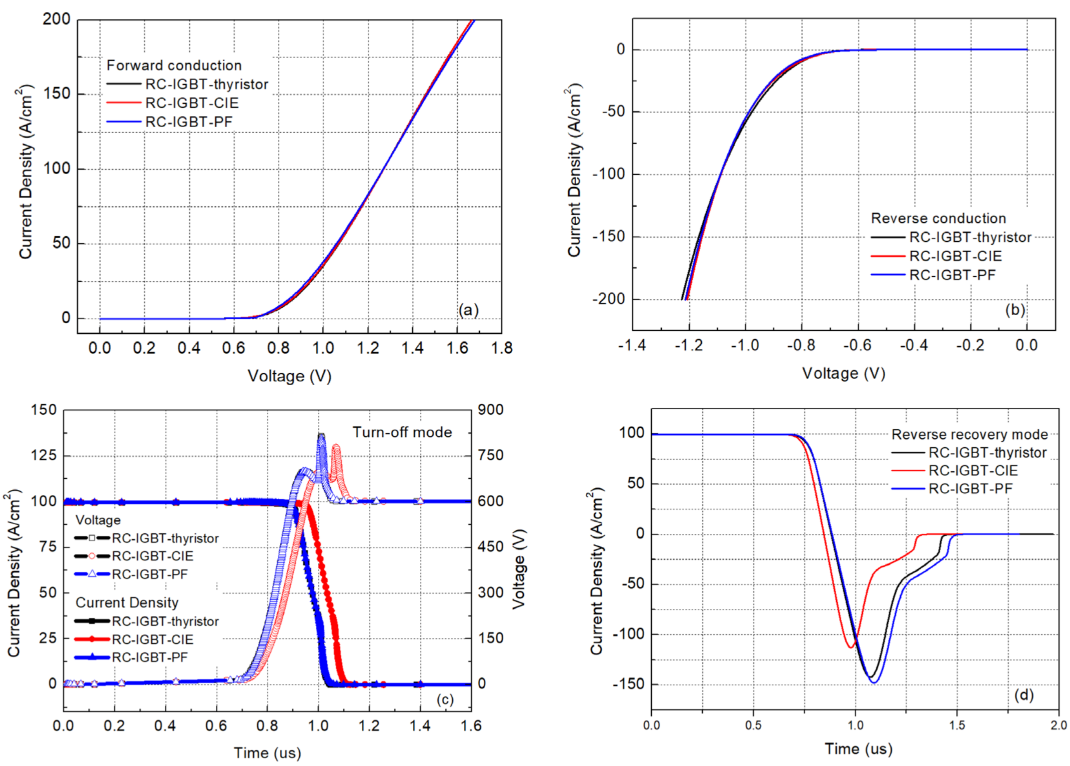

Figure 13. Static and switching characteristics comparison for the proposed RC-IGBT-CIE, conventional RC-IGBT-thyristor and RC-IGBT-PF: (**a**) forward conduction, (**b**) reverse conduction, (**c**) turn-off voltage and current density waveforms, and (**d**) reverse recovery current density waveforms, temperature = 300 K.

In the last section, the isothermal simulations with room temperature T = 300 K were performed. It can be seen from the simulation results that the enhancement of the proposed RC-IGBT-CIE mainly comes from the improvement of the reverse characteristics. Figure 14 shows the reverse characteristics comparison of reverse conduction I–V curves and reverse recovery current density waveforms for the proposed RC-IGBT-CIE and conventional RC-IGBT-thyristor with temperature = 425 K. As seen, the improvement is also observed at a high temperature of T = 425 K.

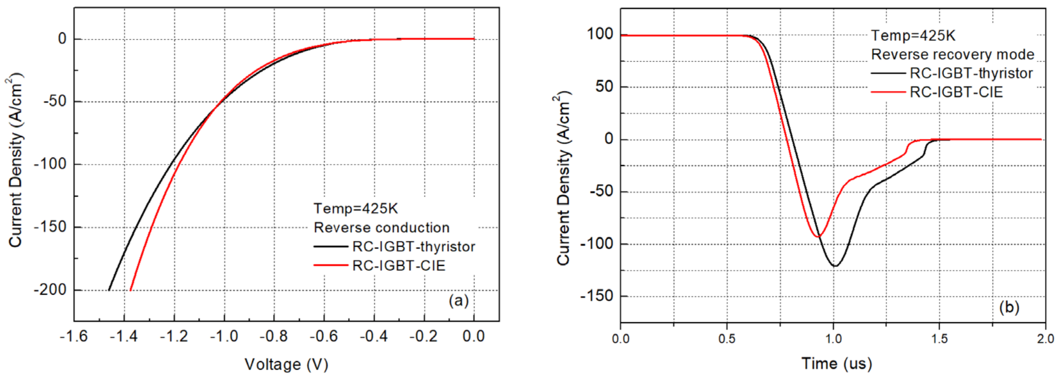

Figure 14. Reverse characteristics comparison for the proposed RC-IGBT-CIE and conventional RC-IGBT-thyristor: (**a**) I–V curves of the reverse conduction, and (**b**) reverse recovery current density waveforms, temperature = 425 K.

5. Conclusions

In summary, a new structure of Collector-side Injection-Enhanced RC-IGBT named RC-IGBT-CIE with low switching loss is proposed and investigated using simulations. The CIE structure enhances the carrier concentration at the collector side of the proposed device in the reverse conduction state, which results in a low reverse-conducting voltage. When compared to the conventional RC-IGBT with anti-parallel thyristor (RC-IGBT-thyristor), with the same total conducting voltage, the lower total switching loss with an inductive load circuit is obtained by using the modified carrier concentration profile which resulted in both the CIE effect and low-injection-efficiency p-emitter. The proposed RC-IGBT-CIE also has good short-circuit capability.

Author Contributions: Conceptualization, W.C.; methodology, W.C. and P.Z.; software, W.C.; data curation, S.Q.; writing—original draft preparation, W.C.; writing—review and editing, W.C.; visualization, K.Z.; funding acquisition, W.C. All authors have read and agreed to the published version of the manuscript.

Funding: This work was supported by Project of Chongqing Natural Science Foundation (No. cstc2020jcyj-msxmX0572), Science and Technology on Analog Integrated Circuit Laboratory Foundation Project, China (No. 6142802200510), and Project Supported by the Fundamental Research Funds for the Central Universities (No. 2020CDJ-LHZZ-076).

Data Availability Statement: Data are contained within the article.

Conflicts of Interest: The authors declare no conflict of interest.

References

1. Takahashi; Yamamoto; Aono; Minato. 1200 V reverse conducting IGBT. In Proceedings of the 16th International Symposium on Power Semiconductor Devices and ICs, Kitakyushu, Japan, 24–27 May 2004; pp. 133–136. [CrossRef]
2. Ruthing, H.; Hille, F.; Niedernostheide, F.-J.; Schulze, H.-J.; Brunner, B. 600 V Reverse Conducting (RC-)IGBT for Drives Applications in Ultra-Thin Wafer Technology. In Proceedings of the 19th International Symposium on Power Semiconductor Devices and IC's, Jeju Island, Republic of Korea, 27–31 May 2007; pp. 89–92. [CrossRef]
3. Rahimo, M.; Schlapbach, U.; Kopta, A.; Vobecky, J.; Schneider, D.; Baschnagel, A. A High Current 3300 V Module Employing Reverse Conducting IGBTs Setting a New Benchmark in Output Power Capability. In Proceedings of the 2008 20th International Symposium on Power Semiconductor Devices and IC's, Orlando, FL, USA, 18–22 May 2008; pp. 68–71. [CrossRef]

4. Chen, W.; Zhang, B.; Li, Z. Area-Efficient Fast-Speed Lateral IGBT with a 3-D n-Region-Controlled Anode. *IEEE Electron Device Lett.* **2010**, *31*, 467–469. [CrossRef]
5. Findlay, E.M.; Udrea, F. Reverse-Conducting Insulated Gate Bipolar Transistor: A Review of Current Technologies. *IEEE Trans. Electron Devices* **2019**, *66*, 219–231. [CrossRef]
6. Reigosa, P.D.; Rahimo, M.; Minamisawa, R.; Iannuzzo, F. Switching Stability Analysis of Paralleled RC-IGBTs with Snapback Effect. *IEEE Trans. Electron Devices* **2021**, *68*, 3429–3434. [CrossRef]
7. Zhu, L.; Rahimo, M.; Luo, H.; Xiao, Q.; Qin, R.; Xiao, H.; Liu, P. Advanced High Voltage Reverse Conducting RC-IGBT Technology with Low Losses and Robust Switching Performance. In Proceedings of the 2020 32nd International Symposium on Power Semiconductor Devices and ICs (ISPSD), Vienna, Austria, 13–18 September 2020; pp. 513–516. [CrossRef]
8. Findlay, E.M.; Udrea, F.; Antoniou, M. Investigation of the Dual Implant Reverse-Conducting SuperJunction Insulated-Gate Bipolar Transistor. *IEEE Electron Device Lett.* **2019**, *40*, 862–865. [CrossRef]
9. Xu, X.; Chen, Z. Simulation Study of a Novel Full Turn-on RC-IGBT with Ultralow Energy Loss. *IEEE Electron Device Lett.* **2019**, *40*, 757–760. [CrossRef]
10. Wang, Z.; Yang, C.; Huang, X. A Novel Concept of Electron–Hole Enhancement for Superjunction Reverse-Conducting Insulated Gate Bipolar Transistor with Electron-Blocking Layer. *Micromachines* **2023**, *14*, 646. [CrossRef] [PubMed]
11. Deng, G.; Luo, X.R.; Wei, J.; Zhou, K.; Huang, L.; Sun, T.; Liu, Q.; Zhang, B. A Snapback-Free Reverse Conducting Insulated-Gate Bipolar Transistor With Discontinuous Field-Stop Layer. *IEEE Trans. Electron Devices* **2018**, *65*, 1856–1861. [CrossRef]
12. Zhang, X.-D.; Wang, Y.; Wu, X.; Bao, M.-T.; Yu, C.-H.; Cao, F. An Improved V_{CE}–E_{OFF} Tradeoff and Snapback-Free RC-IGBT with P^+ Pillars. *IEEE Trans. Electron Devices* **2020**, *67*, 2859–2864. [CrossRef]
13. Li, L.; Li, Z.; Chen, P.; Yang, Y.; Rao, Q.; Wang, T.; Zhao, Y.; Yang, Y.; Ren, M. Actively controlled anode auxiliary gate super-junction insulated gage bipolar transistor with extremely low Eoff. *Semicond. Sci. Technol.* **2023**, *38*, 125001. [CrossRef]
14. Liu, Z.; Sheng, K. A Novel Self-Controlled Double Trench Gate Snapback Free Reverse-Conducting IGBT with a Built-in Trench Barrier Diode. *IEEE Trans. Electron Devices* **2020**, *67*, 1705–1711. [CrossRef]
15. Wu, Z.; He, Y.; Liu, D.; Zhang, C.; Ge, X.; Liu, D. Novel Backside Structure for Reverse Conducting Insulated-Gate Bipolar Transistor with Two Different Collector Trench. *IEEE Trans. Electron Devices* **2022**, *69*, 4414–4420. [CrossRef]
16. Jiang, H.; Zhang, B.; Chen, W.; Li, Z.; Liu, C.; Rao, Z.; Dong, B. A Snapback Suppressed Reverse-Conducting IGBT With a Floating p-Region in Trench Collector. *IEEE Electron Device Lett.* **2012**, *33*, 417–419. [CrossRef]
17. Liu, S.; Tsukamoto, G.; Che, H.; Zhang, S.; Zhang, Z.; Inuishi, M. A Novel 1.2kV Snap-back Suppressed RC-VIGBT with Small Switching Energy Loss and Simple Fabrication Process. In Proceedings of the 2023 7th IEEE Electron Devices Technology & Manufacturing Conference (EDTM), Seoul, Republic of Korea, 7–11 March 2023; pp. 1–3. [CrossRef]
18. Zhang, X.; Gong, M.; Pan, J.; Song, M.; Zhang, H.; Zhang, L. Simulation Study of Low Turn-Off Loss and Snapback-Free SA-IGBT with Injection-Enhanced *p*-Floating Layer. *Electronics* **2022**, *11*, 2351. [CrossRef]
19. Chen, W.; Lin, X.; Li, S.; Huang, Y.; Huang, Y.; Han, Z. A snapback-free reverse-conducting IGBT with multiple extraction channels. *J. Power Electron.* **2021**, *22*, 377–382. [CrossRef]
20. Zhang, X.-D.; Wang, Y.; Bao, M.-T.; Li, X.-J.; Yang, J.-Q.; Cao, F. A Snapback Suppressed *RC*-IGBT With N-Si/n-Ge Heterojunction at Low Temperature. *IEEE Trans. Electron Devices* **2021**, *68*, 5062–5067. [CrossRef]
21. Liu, C.; Wu, G.; Wei, M.; Xu, X.; Xing, P.; Zhang, P.; Sun, R.; Chen, W.; Li, Z.; Zhang, B. A Novel Full Tun-on Reverse-Conducting IGBT with Enhanced Carrier Concentration Modulation in Collector Side. In Proceedings of the 2022 IEEE 16th International Conference on Solid-State & Integrated Circuit Technology (ICSICT), Nangjing, China, 25–28 October 2022; pp. 1–3. [CrossRef]
22. Chen, W.; Huang, Y.; Li, S.; Huang, Y.; Han, Z. A Snapback-Free and Low-Loss RC-IGBT With Lateral FWD Integrated in the Terminal Region. *IEEE Access* **2019**, *7*, 183589–183595. [CrossRef]
23. Hsu, W.C.; Udrea, F.; Hsu, H.; Lin, W. Reverse-conducting insulated gate bipolar transistor with an anti-parallel thyristor. In Proceedings of the 2010 22nd International Symposium on Power Semiconductor Devices & IC's (ISPSD), Hiroshima, Japan, 6–10 June 2010; pp. 149–152.
24. Zhu, L.; Chen, X. A novel snapback-free reverse conducting IGBT with anti-parallel Shockley diode. In Proceedings of the 2013 25th International Symposium on Power Semiconductor Devices & IC's (ISPSD), Kanazawa, Japan, 26–30 May 2013; pp. 261–264. [CrossRef]
25. Suzuki, K.; Yoshida, T.; Haraguchi, Y.; Koketsu, H.; Narazaki, A. Low switching loss diode of 600V RC-IGBT with new contact structure. In Proceedings of the 2021 33rd International Symposium on Power Semiconductor Devices and ICs (ISPSD), Nagoya, Japan, 30 May–3 June 2021; pp. 31–34. [CrossRef]
26. Wu, W.; Li, Y.; Yu, M.; Gao, C.; Shu, Y.; Chen, Y. Low Switching Loss Built-In Diode of High-Voltage RC-IGBT with Shortened P+ Emitter. *Micromachines* **2023**, *14*, 873. [CrossRef]
27. Naito, M.; Matsuzaki, H.; Ogawa, T. High current characteristics of asymmetrical p-i-n diodes having low forward voltage drops. *IEEE Trans. Electron Devices* **1976**, *23*, 945–949. [CrossRef]
28. Porst, A.; Auerbach, F.; Brunner, H.; Deboy, G.; Hille, F. Improvement of the diode characteristics using emitter-controlled principles (EMCON-diode). In Proceedings of the 9th International Symposium on Power Semiconductor Devices and IC's, Weimar, Germany, 26–29 May 1997; pp. 213–216. [CrossRef]

29. Matsudai, T.; Ogura, T.; Oshino, Y.; Naijo, T.; Kobayashi, T.; Nakamura, K. 1200V SC(Schottky controlled injection)-diode, an advanced fast recovery concept with high carrier lifetime. In Proceedings of the 2013 25th International Symposium on Power Semiconductor Devices & IC's (ISPSD), Kanazawa, Japan, 26–30 May 2013; pp. 339–342. [CrossRef]
30. Padmanabhan, K.; Hu, J.; Zhang, L.; Bobde, M.; Guan, L.; Yilmaz, H.; Kim, J. A novel Trench Fast Recovery Diode with injection control. In Proceedings of the 2014 IEEE 26th International Symposium on Power Semiconductor Devices & IC's (ISPSD), Waikoloa, HI, USA, 15–19 June 2014; pp. 23–26. [CrossRef]
31. Gejo, R.; Ogura, T.; Misu, S.; Maeda, Y.; Matsuoka, Y.; Yasuhara, N.; Nakamura, K. High switching speed trench diode for 1200V RC-IGBT based on the concept of Schottky Controlled injection (SC). In Proceedings of the 2016 28th International Symposium on Power Semiconductor Devices and ICs (ISPSD), Prague, Czech Republic, 12–16 June 2016; pp. 155–158. [CrossRef]
32. Kitagawa, M.; Omura, I.; Hasegawa, S.; Inoue, T.; Nakagawa, A. A 4500 V injection enhanced insulated gate bipolar transistor (IEGT) operating in a mode similar to a thyristor. In Proceedings of the IEEE International Electron Devices Meeting, Washington, DC, USA, 5–8 December 1993; pp. 679–682. [CrossRef]
33. Oyama, K.; Kohno, Y.; Sakano, J.; Uruno, J.; Ishizaka, K.; Kawase, D.; Mori, M. Novel 600-V trench high-conductivity IGBT (Trench HiGT) with short-circuit capability. In Proceedings of the 13th International Symposium on Power Semiconductor Devices & ICs. IPSD '01 (IEEE Cat. No.01CH37216), Osaka, Japan, 7 June 2001; pp. 417–420. [CrossRef]
34. Mori, M.; Oyama, K.; Kohno, Y.; Sakano, J.; Uruno, J.; Ishizaka, K.; Kawase, D. A Trench-Gate High-Conductivity IGBT (HiGT) With Short-Circuit Capability. *IEEE Trans. Electron Devices* **2007**, *54*, 2011–2016. [CrossRef]
35. *Taurus Medici User's Guides*; Synopsys, Inc.: Mountain View, CA, USA, 2013.